Roughness of glancing angle deposited titanium thin films: an experimental and computational study

2012 Nanotechnology 23 385708

(http://iopscience.iop.org/0957-4484/23/38/385708)

Nanotechnology **23** (2012) 385708 (7pp) doi:10.1088/0957-4484/23/38/385708

Roughness of glancing angle deposited titanium thin films: an experimental and computational study

Matilda Backholm[1], **Morten Foss**[1] **and Kai Nordlund**[2]

[1] Interdisciplinary Nanoscience Center (iNANO) and Department of Physics and Astronomy, Aarhus University, Ny Munkegade 118, DK-8000 Aarhus C, Denmark
[2] Department of Physics, University of Helsinki, PO Box 64, FI-00014 Helsinki, Finland

E-mail: backhomm@mcmaster.ca

Received 23 May 2012, in final form 31 July 2012
Published 5 September 2012
Online at stacks.iop.org/Nano/23/385708

Abstract
The characterization of roughness at the nanoscale by the means of atomic force microscopy (AFM) was performed on high aspect ratio glancing angle deposited titanium thin films. With the use of scanning electron microscopy as well as x-ray photoelectron spectroscopy, it was shown that the AFM measurements gave rise to incorrect roughness values for the films consisting of the highest aspect ratio structures. By correcting for this experimental artefact, the difference between the saturated roughness value of a film grown with conventional physical vapour deposition and films grown with a glancing angle of deposition was shown to behave as a power law function of the deposition angle, with a saturated roughness exponent of $\kappa = 7.1 \pm 0.2$. This power law scaling was confirmed by three-dimensional molecular dynamics simulations of glancing angle deposition, where the saturated roughness exponent was calculated to $\kappa = 6.7 \pm 0.4$.

(Some figures may appear in colour only in the online journal)

1. Introduction

Modern nanoscience research is interdisciplinary in its attempts to functionalize artificial materials with new unique properties. One example is in the design of biomaterials, where the creation of, e.g., medical implants, such as artificial heart valves and hip joints, is needed to sustain vital body functions or replace structures in the human body [1]. In order for these implants to perform with an appropriate response from the body, the material of the implant needs to be perfectly suited for the specific environment and demands of the host. Titanium has for a long time been known to be such a biocompatible material, and has therefore become one of the most commonly used modern biomaterials for orthopaedic implants, such as artificial hip and dental implants [2, 3].

The surface roughness of biomaterials is a highly contributing factor to the guiding of protein adsorption [4, 5], and will determine the subsequent cellular response to [6–8], as well as the general success, of these [1]. This roughness, often defined as the root-mean-square (rms) fluctuation of the height, w, behaves differently at different length scales, L, and is for the case of self-affine films generally described as [9–11]

$$w(L) \sim \begin{cases} w_{\text{sat}}, & \text{if } L \gg L_{\text{crossover}} \\ L^{\gamma}, & \text{if } L \ll L_{\text{crossover}} \end{cases} \quad (1)$$

where $L_{\text{crossover}}$ is the length at which saturation of the roughness, w_{sat}, occurs, and γ is the so called roughness exponent, describing the power-law-like increase of the roughness at smaller length scales [12].

The detailed characterization of surface roughness is thus a crucial step in the quantification of materials properties, and can easily be performed with various surface sensitive techniques, the most common being atomic force microcopy (AFM). For the case of surfaces with large height variations, however, the geometrical constraints of AFM tips, where the physical width of the tip limits its penetration depth [13], will alter the results gained from such measurements. An example

of such surfaces are glancing angle deposited (GLAD) thin films, consisting of a nanostructure of isolated columns with high aspect ratios, manufactured by depositing atoms at an oblique angle of incidence [14]. AFM has been extensively used to study the roughness of GLAD thin films [12, 15–26].

Here we present the results of roughness measurements performed with AFM on high aspect ratio glancing angle deposited titanium thin films. By the means scanning electron microscopy (SEM) and x-ray photoelectron spectroscopy (XPS) we, furthermore, show how these AFM measurements give rise to erroneous and misleading values of the saturated roughness parameter (shown in equation (1)) for the roughest surfaces. By correcting for the tip-induced effect in the AFM measurements, the accurate relation, Δw_{sat}, between the saturation values for the roughness of GLAD films with respect to a film grown with conventional physical vapour deposition (PVD) is shown to scale as a power law of the deposition angle. This result is confirmed by a three-dimensional molecular dynamics (MD) simulation of glancing angle deposition.

In short, our results show that surface roughness measurements performed with AFM on GLAD surfaces may not give the correct results, and that care should be taken to ensure the validity of AFM measurements on similar high aspect ratio surfaces.

2. Experimental details

2.1. Sample preparation

Polished silicon wafers, cut in the (100) direction ($\pm 0.5°$) and with a diameter of $2''$ (5.08 cm), were used as substrates for the titanium deposition. The initial roughness of these wafers was estimated to be on the subnanometer scale. Prior to deposition, the wafers were cleaned from organic contamination in a UV–ozone cleaner (BioForce, Ames, IA) for 30 min and blown clean with nitrogen gas to remove dust.

Titanium (from Goodfellow; high purity of 99.99%) was deposited by electron beam evaporation at room temperature (approx. 300 K) with an initial chamber pressure of 3×10^{-7} Torr. The distance between the source and the centre of the sample was 300 mm and the source diameter was smaller than 10 mm. The total error in the deposition angle was estimated to be $\pm 1.5°$.

Four different deposition angles, defined as the angle between the direction of the incoming atoms and the normal to the surface, were used: $\alpha = 0°$, $55°$, $80°$, and $85°$. Furthermore, the sample was rotated during the deposition with a rotational speed of $\varphi = 10$ rpm, giving rise to the growth of vertical columns on the surface.

The film deposited at normal incidence was grown at a rate of 0.5 nm s^{-1} and was made to be 50 nm thick. This nominal thickness was controlled by Quartz Crystal Microbalance (QCM) measurements using a mass density of $\rho = 4.5$ g cm^{-3}, corresponding to the bulk value for titanium. A correction in deposition time due to the change in effective surface area for non-normal incidence was performed. Due to the smaller surface mass density for the samples grown at oblique angles, the actual film thickness of these films increased as a function of deposition angle for films of similar mass [12], and was thus much thicker than what the nominal thickness measured by the QCM suggested.

2.2. Atomic force microscopy

Atomic force microscopy measurements were performed with a Nanoscope IIIa Multimode SPM (Veeco Instruments, Santa Barbara, CA, USA), and an Agilent 5500 AFM (Agilent Technologies, Chandler, AZ, USA). The scans were performed in tapping mode in ambient conditions with a scan rate of 1 line s^{-1}, and a series of images with the linear dimensions of 0.5, 1, 5.5, and 10 μm, and the resolution of 512 pixels $\times$ 512 pixels were recorded at several different locations on the sample. The thickness, length, and width of the silicon cantilevers (OLYMPUS Micro Cantilever AC 160TS) were 4.6 μm, 160 μm, and 50 μm, respectively. The spring constant and resonance frequency were around 42 N m^{-1} and 300 kHz, respectively, and the probes had a height of 11 ± 4 μm, a tip radius below 10 nm, and a half cone angle of $18°$.

Analysis of the AFM data was performed with the image analysis software package Scanning Probe Image Processor (SPIP, Image Metrology A/S, Denmark), and the apparent roughness of the films was calculated at different length scales of the AFM images with a customized extension for this program.

2.3. Scanning electron microscopy

Scanning electron microscopy measurements were performed with a Nova NanoSEM 600 (FEI Company, Oregon, USA), imaging secondary electrons with the use of ET and TL detectors. The voltage and spot size was kept at 5 kV and 3 kV, respectively, whereas the aperture size was 30 μm. A magnification of up to 250 000$\times$was used when imaging the samples, which were kept in a chamber with a pressure around 0.2 mPa.

2.4. X-ray photoelectron spectroscopy

The XPS measurements were performed with a Kratos Axis Ultra XPS (Kratos Analytical Ltd, UK). The x-ray source was driven with a power of 150 W (Anode voltage: 15 kV, Emission current: 10 mA) using aluminum, with an emission line at Al $K\alpha_{1,2} = 1486.6$ eV, as the anode material. In the measurements, the pass energy, spot size, and electron take off angle were 160 eV, 700×300 μm^2, and $90°$ (normal to the surface), respectively, and a charge neutralizer was used. At least two spots per sample were analysed in order to account for statistical variations. The calibration was done according to the C 1s peak and the final data was analysed with the processing software CasaXPS.

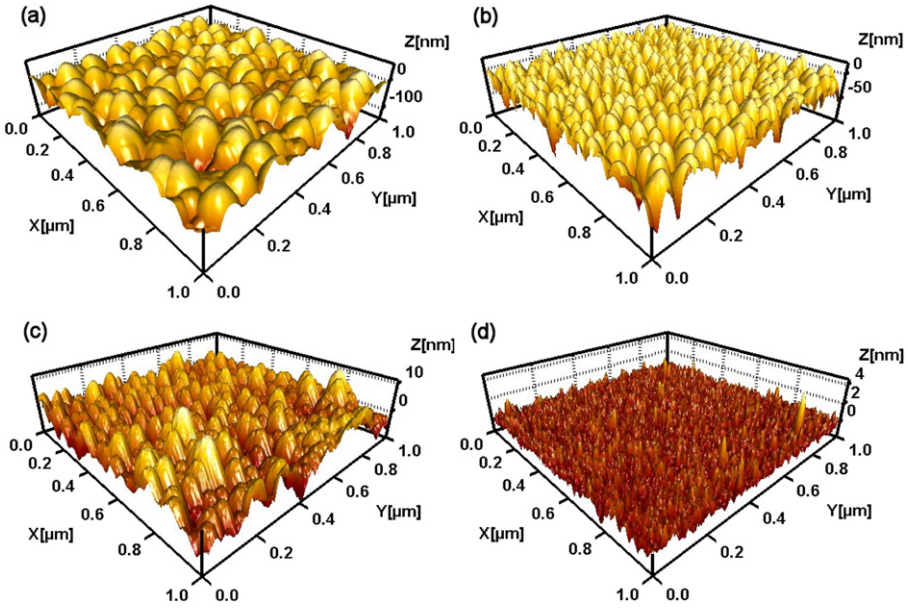

Figure 1. 3D AFM images of the titanium samples produced with the deposition angle (a) $\alpha = 85°$, (b) $\alpha = 80°$, (c) $\alpha = 55°$, and (d) $\alpha = 0°$. Note the different height scales of the images.

2.5. Molecular dynamics simulations

The molecular dynamics simulations were performed with the MD code PARCAS [27]. To simulate titanium, the Ti part of the Sabochick–Lam CuTi-potential was used [28]. A four monolayer thick titanium surface was created with the size 123.12 × 121.79 Å^2, corresponding to 2016 atoms per monolayer, i.e., 8064 atoms in the substrate in total. Periodic boundary conditions were introduced in the directions parallel to the surface to simulate an infinite surface. The two bottom atom layers were fixed, and temperature control was applied on the two atom layers above it, allowing for energy loss to a larger system representing a bulk substrate. Temperature control was also applied at the borders of the substrate. The simulations were performed at 300 K.

In the beginning of the simulation (after 10 fs), a titanium atom was created at a random point 6.5 Å above the highest point of the surface, and an energy of 0.04 eV was given to it in the direction corresponding to deposition at an angle α. The total simulation time per deposited atom was 30 ps, with a time step of less than 4 fs. A total number of 10 000 atoms were deposited. After each deposited atom, the direction of the following incoming ion was rotated one degree, corresponding to a rotational speed of 0.03° ps^{-1}, or 5.6 × 10^9 rpm. The computational deposition flux was 2.24 × 10^8 atoms nm^{-2} s^{-1}, making the ratio between rotational speed and deposition flux similar to that achieved experimentally.

The simulations were performed with the deposition angles $\alpha = 85°$, 80°, 55°, and 0°, and in total 12 simulations were run, corresponding to three simulations with different random seed numbers per angle to account for statistical variations.

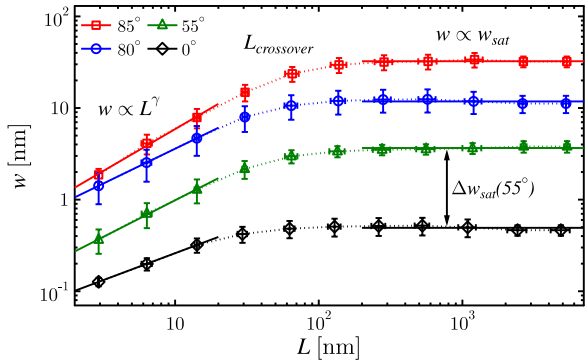

Figure 2. The root-mean-square roughness as a function of the length scale L based on the AFM measurements of the different GLAD films. The scaling of the curves for the different length scale regions is predicted in equation (1). $\Delta w_{sat}(\alpha)$ is the difference between the saturated roughness of a GLAD film ($\alpha > 0°$) and the film grown with conventional PVD ($\alpha = 0°$). The error bars are standard deviations from scans performed on several different samples.

3. Results and discussion

The nanotopographical features of the glancing angle deposited titanium thin films were investigated with atomic force microscopy. Typical three-dimensional AFM images are shown in figure 1, where vertical columns cover the surfaces produced with the larger deposition angles. The topographical variations of the film produced at an angle normal to the surface ($\alpha = 0°$), corresponding to conventional physical vapour deposition, is, as expected, very small in comparison to the films produced at glancing angles of incidence.

The roughness of the different GLAD films was calculated as a function of length scale, and is shown in figure 2.

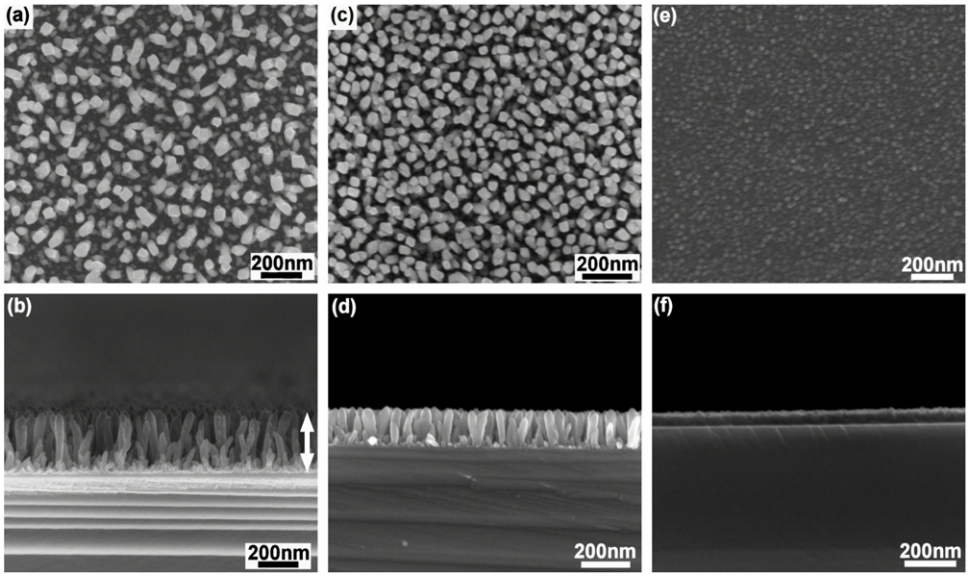

Figure 3. SEM images taken from the top (top) and the side (bottom) of the samples, produced with deposition angles (a)–(b) $\alpha = 85°$, (c)–(d) $\alpha = 80°$, and (e)–(f) $\alpha = 55°$. As shown by the arrow in (b), the film thickness is defined as the distance between the substrate/film and film/air interfaces.

As has already been reported [12], the scaling of the roughness for GLAD films follows the expected trend described by equation (1), where the roughness scales as a power law for smaller length scales, whereas a saturation in the roughness is seen for length scales larger than $L_{\text{crossover}}$. The relation between the saturated roughness value, $w_{\text{sat}}(\alpha)$, for GLAD films with respect to the film grown with conventional PVD ($\alpha = 0°$) is illustrated for the $\alpha = 55°$ case in figure 2, and is here defined as

$$\Delta w_{\text{sat}}(\alpha) = w_{\text{sat}}(\alpha) - w_{\text{sat}}(0°). \quad (2)$$

Scanning electron microscopy measurements were performed on the same GLAD films as investigated with AFM, and the result is shown in figure 3 from both surface and cross-sectional views. The high aspect ratio vertical columns, with columnar width versus height fractions as low as 0.2, produced at most grazing angles ($\alpha = 85°$ and $80°$) are a result of the fast rotation of the samples during deposition, and were desired features in the manufacturing of these nanorough surfaces.

From figure 3, the total film height can be determined as: $h_{\text{SEM},\alpha=85°} = 315 \pm 10$ nm, $h_{\text{SEM},\alpha=80°} = 145 \pm 5$ nm, and $h_{\text{SEM},\alpha=55°} = 60 \pm 2$ nm. The film produced with normal incidence PVD, i.e., with $\alpha = 0°$, is not shown in the figure due to the extremely small topographical variations, already noticed in figure 1(d). The thickness of this film corresponded to the nominal film thickness (50 nm) set in the deposition.

X-ray photoelectron spectroscopy measurements were performed on the different samples to investigate the variation of atomic concentrations as a function of deposition angle. The results from these measurements are tabulated in table 1, where the concentrations of carbon, oxygen, titanium, and silicon are shown. The presence of the two former materials on the surface was expected, since the samples were stored in ambient conditions after the deposition, whereas the small amount of nitrogen found on all of the samples (not shown in the table) was believed to be due to the binding of pure titanium with residual gas nitrogen present in the vacuum chamber during deposition. An increased silicon signal, originating from the substrate beneath the titanium films, points towards a more open structure for the two roughest GLAD films and indicates that the columns span the entire thickness of the film, leaving open voids penetrating nearly all the way down to the substrate of the thin films.

Table 1. Atomic concentration, as determined by XPS, for samples deposited at different deposition angles, α. The concentration of carbon and titanium is inversely correlated, whereas the atomic concentration of nitrogen and oxygen remains more or less constant for the different values of α. The presence of silicon on the surfaces is explained by the silicon wafer beneath the thin titanium film, and the increase of its atomic concentration with the deposition angle corresponds to the surface becoming rougher for more glancing angles. Also a small amount of nitrogen was present on the surface (not shown here). The errors are standard deviations from several measurements.

α (deg)	C 1s	O 1s	Ti 2p	Si 2p
85	27.0 ± 0.4	50.6 ± 1.3	16.9 ± 1.3	3.5 ± 1.6
80	26.7 ± 1.0	51.4 ± 0.5	18.9 ± 0.2	1.0 ± 0.8
55	24.0 ± 1.0	51.5 ± 0.5	21.6 ± 1.4	0.3 ± 0.4
0	18.3 ± 0.6	54.6 ± 0.4	26.2 ± 0.8	0.6 ± 0.5

By comparing the dimensions of the columns in figures 1 and 3, the geometrical constraints of the AFM measurements can be seen as both a tip broadening effect, where the apparent width of the columns is increased, as well as a substantial decrease in the measured height of the films. This vertical effect caused by the low aspect ratio of the AFM tip is best visualized in line scans taken in the fast scan direction of the AFM images of the different samples, as shown in figure 4. In this figure the absolute height of the films has been corrected with the help of the film thickness results gained from the

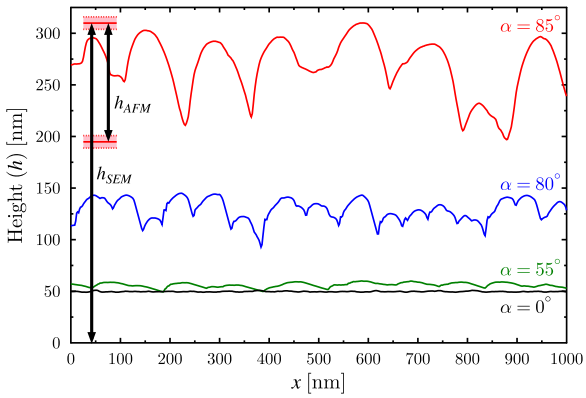

Figure 4. AFM line scans of the samples in the fast scan direction. The thickness of the $\alpha = 0°$ sample is set to be 50 nm in the deposition, and the offsets for the three largest angles correspond to the height measured with SEM (figure 3). The limitations in the AFM tip penetration depth is visible as only a smaller part, h_{AFM}, defined as the peak-to-valley distance, is probed as compared to the total film height measured with SEM, h_{SEM}. The error bars in the height measurements come from the analysis of several line scans of different samples.

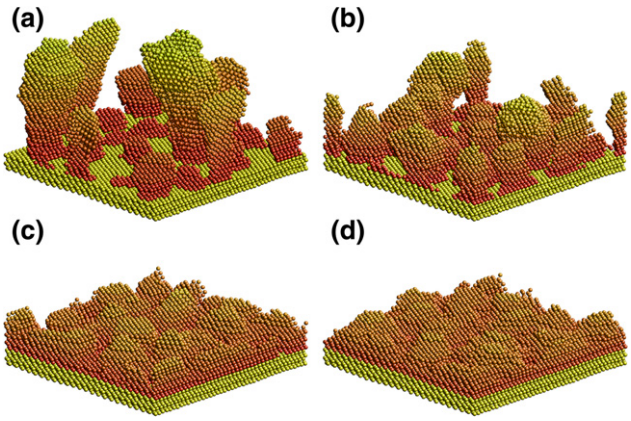

Figure 5. Snapshots from the molecular dynamics simulations showing the structure of the thin films, consisting of 10 000 titanium atoms deposited on a titanium substrate at a deposition angle of (a) $\alpha = 85°$, (b) $\alpha = 80°$, (c) $\alpha = 55°$, and (d) $\alpha = 0°$. The length of the substrate is 12 nm and the colour scheme is chosen to illustrate the height variations.

SEM measurements, and it is obvious that the AFM tip is only able to probe a small fraction (h_{AFM}) of the whole film thickness (h_{SEM}) for the films grown with the two largest deposition angles.

To correct for this experimental artefact, which subsequently also will give rise to erroneous roughness values, a height correcting factor, η, is introduced in order to rescale the variation in film height to the level estimated by SEM. This height correcting factor is defined as

$$\eta(\alpha) = \frac{h_{\mathrm{SEM}}(\alpha)}{h_{\mathrm{AFM}}(\alpha)}, \tag{3}$$

and can be derived from roughness equations by using the general definition of the rms roughness, i.e., how much the film thickness $h(\mathbf{r})$ deviates from the mean thickness $\bar{h}$, or [11]

$$w(L) = \sqrt{\frac{1}{L^2}\sum[h(\mathbf{r}) - \bar{h}]^2}, \tag{4}$$

where L is the linear size of the surface and the mean value of the height is

$$\bar{h} = \frac{1}{L^2}\sum h(\mathbf{r}). \tag{5}$$

The η-corrected saturated roughness value, that is the real value of the roughness at length scales larger than $L_{\mathrm{crossover}}$, is then

$$w^*_{\mathrm{sat}}(\alpha) = \eta(\alpha) w_{\mathrm{sat}}(\alpha). \tag{6}$$

The numerical values of the height correcting factors for the films grown with the largest deposition angles are here determined to be $\eta(85°) = 2.5 \pm 0.2$ and $\eta(80°) = 2.6 \pm 0.2$, where the error is the standard deviation of several AFM and SEM measurements performed on different samples, and account for statistical variations between the films, as well as errors associated with the measurement techniques, and small deviations in the geometries of our standard tip type. If the aspect ratio of the columns were to decrease or the inter-columnar distance were to increase, the AFM tip would be able to probe a larger fraction of the total film height (h_{SEM}), which subsequently would affect both the saturated roughness value, w_{sat}, and the height correcting factor, η. As this change is inversely proportional, it would not, however, affect the value for the corrected surface roughness in equation (6). Since the AFM tip was able to probe the entire height of the two smoothest films, the height correction factors for these surfaces were determined to be, within error, unity.

To gain a better understanding of the roughness of GLAD thin films, we performed three-dimensional molecular dynamics simulations of glancing angle deposition with the same deposition angles as used experimentally, and with a rotational speed giving rise to vertical columns on the surface. Snapshots of the resulting thin films from the simulations are shown in figure 5, where structurally very similar columnar features have been produced, as compared to those seen experimentally in figures 1 and 3. The side length of each substrate is approximately 12 nm, and a correlation between the computational and experimental surfaces and roughness calculations, clearly spanning different length scales, is justified by the self-affine properties of the GLAD films [12].

Surface roughness was calculated for different length scales in the same manner as done experimentally, with the difference that the entire thickness of the simulated films could be accounted for. The result is shown in figure 6, where the same scaling of the roughness, predicted by equation (1), is seen as for the experimental results in figure 2.

The biggest difference between the experimental and computational roughness, that is, the difference between the results in figures 2 and 6, is the relation between the saturated values of the roughness as a function of deposition angle. This relation, defined as $\Delta w_{\mathrm{sat}}(\alpha)$ in equation (2) and illustrated in figure 2, is plotted in figure 7 for both the experimental (circles) and computational (triangles) case.

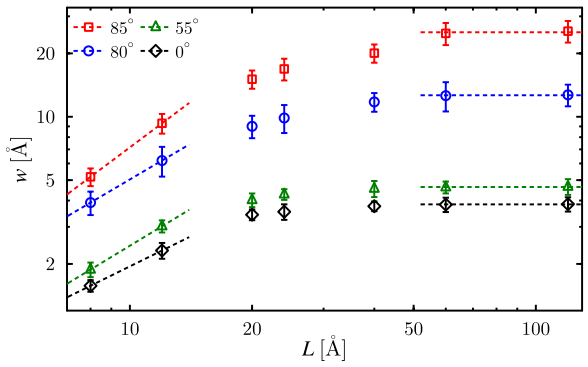

Figure 6. The root-mean-square roughness as a function of the length scale L of thin GLAD films produced computationally with different deposition angles. The dashed lines indicate the functional behaviour predicted by equation (1), and the error bars are standard deviations from the three different simulations performed per deposition angle.

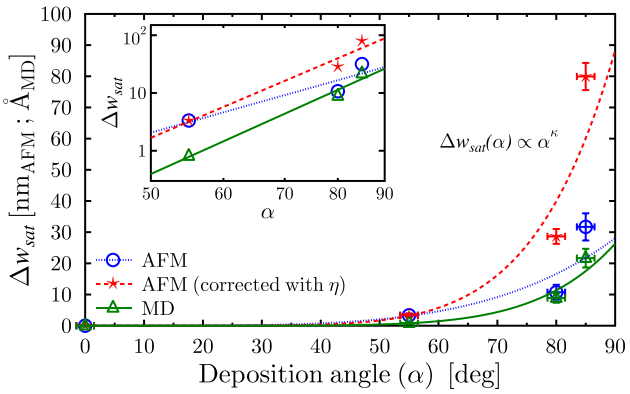

Figure 7. The difference between the saturated roughness values for the film grown with conventional PVD ($\alpha = 0°$) and GLAD films ($\alpha > 0°$) as a function of deposition angle. Power law functions have been fitted to the experimental (both original and corrected AFM results) and computational (MD) data, which is also shown in the inset, where logarithmic axes have been used to emphasize the power law behaviour, and the error bars have been removed for clarity. The unit on the y-axis is nm for the AFM results, and Å for the MD results.

By fitting lines to the data in figure 7, Δw_{sat} can be shown to be a power law function of the deposition angle for the computational case, which is seen more clearly in the inset in figure 7, where the same data is plotted with logarithmic axes. This power law behaviour can be expressed analytically as

$$\Delta w_{\mathrm{sat}}(\alpha) \propto \alpha^{\kappa}, \tag{7}$$

where κ is introduced as a saturated roughness exponent. The values for κ as well as the R^2 values for the power law fits are shown in table 2.

From the values in table 2, it becomes clear that the power law fit is not very successful for the AFM results. This is due to the already mentioned failure in probing the entire thickness of the roughest thin films with AFM. By using the η-correction for the saturated roughness of the two roughest films as defined in equation (6), that is, by multiplying $\eta(\alpha)$ with the corresponding saturated roughness values, the dashed line in figure 7 is the result. As is seen in the inset as well as in table 2, the power law function of the corrected AFM data is in very good agreement with the computational results, with, within error, the same saturated roughness exponent as was found in the MD simulations.

The introduction of a height correcting factor, η, can thus successfully rescale the roughness values of films produced with glancing angles of incidence, which in this way exhibit the same power law behaviour of $\Delta w_{\mathrm{sat}}(\alpha)$ as predicted theoretically.

Table 2. The saturated roughness exponent for the computational and experimental films, where both the original and height corrected (*) values are shown. The R^2 values show the quality of the power law fits in figure 7.

Method	κ	R^2 value for fit
MD	6.7 ± 0.4	0.98
AFM	4.4 ± 0.2	0.87
AFM*	7.1 ± 0.2	0.96

4. Conclusions

In this work, we have presented a detailed study of nanoroughness with atomic force microscopy, and shown, by comparison with scanning electron microscopy and x-ray photoelectron spectroscopy, how this method fails to quantify the correct roughness of high aspect ratio titanium films produced with glancing angle deposition. A height correcting factor η was introduced to rescale the saturated value of the roughness for films grown with the most grazing angles of deposition, and the difference, $\Delta w_{\mathrm{sat}}(\alpha)$, between the corrected saturated roughness values of films grown with conventional physical vapour deposition and with glancing angle of incidence was shown to scale as a power law function of deposition angle, with a saturated roughness exponent of $\kappa_{\mathrm{AFM}*} = 7.1 \pm 0.2$. This finding was confirmed by molecular dynamics simulations, where the saturated roughness exponent was calculated to be $\kappa_{\mathrm{MD}} = 6.9 \pm 0.4$. The good agreement between experimental and computational films shows the strength of MD in characterizing similar nanoscale structures.

The power law behaviour introduced here for the increase in the saturated roughness value, w_{sat}, as a function of deposition angle in GLAD thin films can in the future be used to verify the correctness of roughness measurements performed with AFM, which is of the greatest importance when quantifying the surface properties of these films. This power law scaling also contributes with new insight into the broader concept of surface roughness.

Acknowledgments

M Backholm gratefully acknowledges the financial support from the Swedish Cultural Foundation in Finland. The authors also would like to thank Folmer Lyckegaard for the production of the thin films used in this work. Grants of computer time from the CSC Center for Scientific Computing in Espoo, Finland, are gratefully acknowledged.

References

[1] Kasemo B 2002 *Surf. Sci.* **500** 656
[2] van Noort R 1987 *J. Mater. Sci.* **22** 3801
[3] Helsen J A and Breme H J 1998 *Metals as Biomaterials* (New York: Wiley)
[4] Roach P, Ferrar D and Perry C C 2005 *J. Am. Chem. Soc.* **127** 8168
[5] Rechendorff K, Hovgaard M B, Foss M, Zhdanov V P and Besenbacher F 2006 *Langmuir* **22** 10885
[6] Lord M S, Foss M and Besenbacher F 2010 *Nano Today* **5** 66
[7] McNamara L E, McMurray R J, Biggs M J P, Kantawong F, Oreffo R O C and Dalby M J 2010 *J. Tissue Eng.* **1** 120623
[8] Dalby M J, Yarwood S J, Riehle M O, Johnstone H J H, Afforssman S and Curtis A S G 2002 *Exp. Cell Res.* **276** 1
[9] Bellac D L, Niklasson G A and Granqvist C G 1995 *Europhys. Lett.* **32** 155
[10] Family F and Vicsek T 1985 *J. Phys. A: Math. Gen.* **18** 75
[11] Barabasi A-L and Stanley H E 1995 *Fractal Concepts in Surface Growth* (Cambridge: Cambridge University Press)
[12] Dolatshahi-Pirouz A, Hovgaard M B, Rechendorff K, Chevallier J, Foss M and Besenbacher F 2008 *Phys. Rev.* B **77** 115427
[13] Villarrubia J S 1994 *Surf. Sci.* **321** 287
[14] Robbie K, Friedrich L J, Dew S K and Brett M J 1995 *J. Vac. Sci. Technol.* A **13** 1032
[15] Kennedy S R and Brett M J 2003 *Appl. Opt.* **42** 4573
[16] Lintymer J, Gavoille J, Martin N and Takadoum J 2003 *Surf. Coat. Technol.* **174/175** 316
[17] Ruthe K and Barnett S 2003 *Surf. Sci.* **538** L460
[18] Rechendorff K, Hovgaard M B, Chevallier J, Foss M and Besenbacher F 2005 *Appl. Phys. Lett.* **87** 073015
[19] Wang S, Fu X, Xia G, Wang J, Shao J and Fan Z 2006 *Appl. Surf. Sci.* **252** 8734
[20] Lifshitz Y, Edrei R, Hoffman A, Grossman E, Lempert G, Berthold J, Schultrich B and Jager H 2007 *Diamond Relat. Mater.* **16** 1771
[21] Morrow P, Tang X-T, Parker T C, Shima M and Wang G-C 2008 *Nanotechnology* **19** 065712
[22] Lintymer J, Martin N, Chappe J-M and Takadoum J 2008 *Wear* **264** 444
[23] Dolatshahi-Pirouz A, Pennisi C P, Skeldal S, Foss M, Chevallier J, Zachar V, Andreasen P, Yoshida K and Besenbacher F 2009 *Nanotechnology* **20** 095101
[24] Thomas S, Al-Harthi S H, Ramanujan R V, Bangchuan Z and Yan L 2009 *Appl. Phys. Lett.* **94** 063110
[25] Pennisi C P, Dolatshahi-Pirouz A, Foss M, Chevallier J, Fink T, Zachar V, Besenbacher F and Yoshida K 2011 *Colloids Surf.* B **85** 189
[26] Gonzalez-Garcia L, Parra-Barranco J, Sanchez-Valencia J R, Barranco A, Borras A, Gonzalez-Elipe A R, Garcia-Gutierrez M-C, Hernandez J J, Rueda D R and Ezquerra T A 2012 *Nanotechnology* **23** 205701
[27] Nordlund K 2010 PARCAS computer code. The main principles of the molecular dynamics algorithms are presented in [29, 30]
[28] Sabochick M J and Lam N G 1991 *Phys. Rev.* B **43** 5243
[29] Nordlund K, Ghaly M, Averback R S, Caturla M, Diaz de la Rubia T and Tarus J 1998 *Phys. Rev.* B **57** 7556
[30] Ghaly M, Nordlund K and Averback R S 1999 *Phil. Mag.* A **79** 795